

Research paper

# The distribution of otolith polarization vectors in mammals: Comparison between model predictions and single cell recordings

R. Jaeger<sup>a,\*</sup>, A.V. Kondrachuk<sup>b</sup>, T. Haslwanter<sup>c</sup>

<sup>a</sup> Department of Theoretical Astrophysics, University of Tübingen, Auf der Morgenstelle 10, 72076 Tübingen, Germany

<sup>b</sup> Department of Theoretical Physics, Institute of Physics, National Academy of Sciences of Ukraine, 46 Prospekt Nauki, Kiev 03028, Ukraine

<sup>c</sup> Upper Austrian University of Applied Sciences, and Upper Austrian Research, Department for Medical Informatics, Garnisonstr. 21, A-4020 Linz, Austria

Received 31 August 2006; received in revised form 2 January 2008; accepted 15 January 2008

Available online 20 January 2008

## Abstract

The transformation of head-movements into neural signals represents a multi-stage process. It depends on orientation and movement of the head, the geometry and mechanics of the vestibular sensors, and the ensuing processing of the peripheral vestibular signals. While this process is well understood for the semicircular canals, where each canal transduces the angular velocity in the corresponding canal plane, the contributions of the individual otoliths, our linear acceleration sensors, are still under debate. This is in part due to the complex geometrical structure of the otoliths. To improve our understanding of the otoliths, we have developed a new technique to visualize otolith function: using measured 3D-shapes of human otoliths and the observed 2D patterns of hair cell orientation over the epithelia, morphological polarization vectors are predicted. To visualize the geometric distribution of these vectors, we have created distribution plots which indicate the density of hair cell polarization vectors for the different directions. In many respects, our results closely agree with earlier recordings of polarization vectors of vestibular afferents in squirrel monkeys: for example, hair cells on the saccule do not cover the sagittal plane equally, but show a strong concentration in the dorso-ventral directions. Some discrepancies exist in the density distribution of otolith, which could provide valuable information for future anatomical investigations of the otoliths.

© 2008 Published by Elsevier B.V.

**Keywords:** Otolith; Hair cells; Vestibular; Modeling

## 1. Introduction

In all mammals, linear accelerations of the head are sensed by the otolith organs, utricle and saccule, which are located in the inner ear labyrinth. The transformation of the acceleration stimulus into neural signals, carried

out by these sensory organs, represents a complex multi-stage process. Central to this process are the hair cells, which change their membrane potential if small hair bundles, located in the apical part of the cells are tilted. Along with other cell types, hair cells are embedded in the otolith epithelia, a sensory structure completely covered by the otolith membrane. Observations suggest that the tips of the hair bundles are mechanically linked to the otolith membrane (Kachar et al., 1990), which is deformed by accelerations of the head due to embedded high-density otoconia crystals. The membrane potential of a hair cell is determined by tilt direction and displacement magnitude of the hair bundle (Shotwell et al., 1981). The unique direction leading to a maximum depolarization of the cell is

*Abbreviations:* 2D, two dimensional; 3D, three dimensional; MRL, morphological reversal line; **R**-sphere, sphere with radius **R**

\* Corresponding author. Tel.: +49 (7071) 29 78654; fax: +49 (7071) 29 5889.

*E-mail addresses:* [rudijaeger@yahoo.com](mailto:rudijaeger@yahoo.com) (R. Jaeger), [kondr@kondr.kiev.ua](mailto:kondr@kondr.kiev.ua) (A.V. Kondrachuk), [Thomas.Haslwanter@fh-linz.at](mailto:Thomas.Haslwanter@fh-linz.at) (T. Haslwanter).

called “polarization direction” and commonly characterized by a morphological polarization vector. Since the epithelia are not planar structures but curved in 3D-space (Takagi and Sando, 1988; Curthoys et al., 1999), maximum depolarization directions are appropriately represented by 3D-vectors.

Morphological polarization vectors can be determined visually from geometrical aspects of the hair bundles. Using this property, it was found that they are not randomly distributed over the epithelia but form distinct patterns (Lindeman, 1969): the polarization vectors vary smoothly over the epithelium, but reverse direction along the “morphological reversal line” (MRL, solid lines in Fig. 1). The MRL lies within the striola, a band-like region dividing the epithelium.

Hair cells are innervated by bipolar neurons of the vestibular nerve. These afferent fibers generally make contacts with more than one hair cell (Fernandez et al., 1990), and the cells contributing to a particular fiber are called its “ter-

минаl field”. While hair cells are characterized by “morphological polarization vectors”, a “functional polarization vector” can be attributed to a vestibular fiber. This vector describes the direction of an acceleration stimulus which leads to a maximum neural response in the fiber.

The mechanisms underlying the formation of afferent signals have enjoyed a longstanding interest (Ross, 1985; Goldberg et al., 1990b; Sans et al., 2001; Holstein et al., 2004). One aspect of this process is the creation of the functional polarization vector. Thereby these vectors are usually described in a head fixed coordinate system (Fernandez and Goldberg, 1976a), while morphological vectors are depicted with respect to their position on the epithelium (Lindeman, 1969). Goldberg et al. tried to merge the two representations by employing intra-axonal labeling techniques to afferent fibers (Goldberg et al., 1990b). By first measuring functional vectors and reconstructing the position of the corresponding terminal fields on the epithelium, they found that “there is reasonable correspondence between morphological and functional vectors”. This observation was made by comparing measured 2D-vectors with qualitative findings by Lindeman (1969). It was also found that there are some units with functional polarization vectors which were not consistent with the morphological vectors. The measurements by Goldberg et al. provide a thorough description of vestibular afferents, i.e. functional polarization vector and the corresponding location of the terminal field. In contrast, recordings from the vestibular nerve are usually restricted to the measurement of the direction of the functional vectors, and a comparison with the morphological vectors, which are determined by their location on the epithelium, is not possible. To fill this gap, this investigation models the distribution of morphological polarization vectors based on the 3D-curvature of the epithelia and the observations by Lindeman. Central to the linkage between these two aspects is the assumption that morphological polarization vectors lie in tangent planes to the epithelia (Kondrachuk, 2001). This assumption is supported by the finding that head accelerations leading to pure shear displacements of the otolith membrane are the most effective stimulus, and that accelerations perpendicular to the epithelium yield no or only small responses in the vestibular nerve (Fernandez and Goldberg, 1976b).

Using this approach, it becomes feasible to investigate the effects of processing involved with the formation of the functional polarization vectors without employing complex techniques like intra-axonal labeling. Since the data used in this investigation stems from different species and evidence exists that there are substantial variations between otolith organs, even within the same species (Curthoys et al., 1999; Tribukait and Rosenhall, 2001), we are cautious about drawing conclusions with regard to polarization vector processing. Nevertheless, based on the differences between measured and modeled vectors, problems associated with measurement of functional vectors and their effects can be identified.

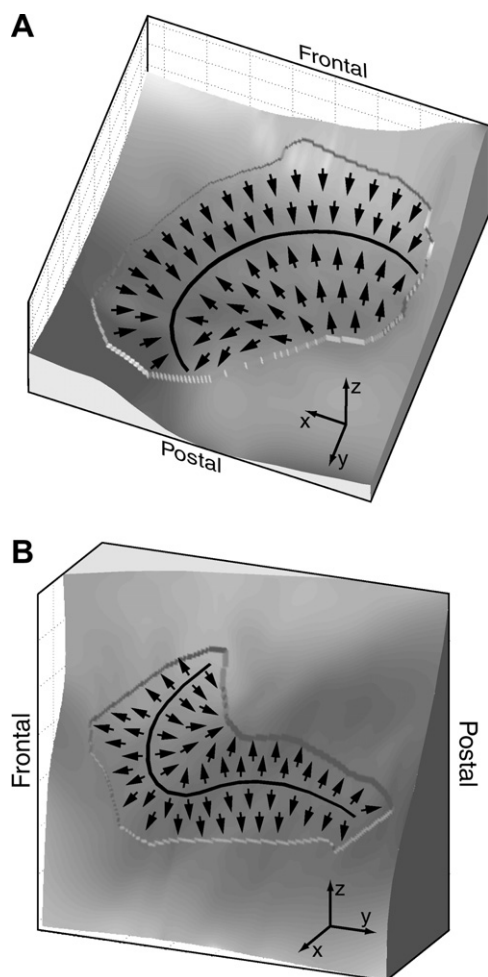


Fig. 1. View of the macular surfaces of left utricle (A), and sacculle (B). Arrows indicate the pattern of morphological polarization vectors while the thick black lines show the location of the MRL. Regions that represent measured data are slightly elevated with respect to the remaining surface. The insets illustrate the orientation of the respective coordinate system:  $x/y/z$  indicates left/back/up, respectively.

## 2. Methods

To determine the morphological polarization vectors, the local orientation of the epithelia surfaces are required. These surfaces were obtained from measurements by Takagi and Sando (1988). In their experiments, human labyrinths were fixated, sliced, digitized, and reconstructed in the computer. The resulting data sets represent the curved surfaces of the epithelia as well as other parts of the inner ear labyrinth. Structurally, the data sets are organized in several groups, with each group corresponding to data points along the edge of one labyrinth slice. Since the investigation by Takagi and Sando focused on the otoliths, saccular and utricular epithelia were measured with a high spatial resolution. While it is commonly assumed that epithelia surfaces are smooth, the measurement process can introduce geometric artifacts that lead to surfaces with large local slopes. As a result, the surfaces look “bumpy”. As this investigation tries to determine tangent vectors of the epithelia, smooth representations of the surfaces were particularly important, and the data sets were pre-processed to remove artifacts of the measurement process: single data rows that appeared misplaced were shifted or rotated by small amounts to align with the others; some rows that appeared deformed and did not fit in with the rest of the data were discarded. The resulting data sets were represented on a regular grid. If the grid is for example in the  $x$ - $y$ -plane, corresponding  $z$ -values that describe the epithelia surfaces were calculated by interpolating between the surrounding measured points. Due to the regular grid, the surfaces are represented with small quadrilaterals. Additional data points were introduced outside the measured epithelia areas, to provide a smooth, clearly curved continuation for the graphical representation. Remaining artifacts of the slicing procedure were removed by smoothing the surfaces with a Savitzky–Golay filter (Press et al., 1992). A visual inspection ensured that only artifacts were removed. The calculations were done using MATLAB (The MathWorks, Natick, Mass., USA).

The surfaces of the epithelia were represented with respect to a coordinate system that allowed simple comparison with existing observations. We employed the system used by Fernandez and Goldberg (1976a). In this coordinate system, the  $x$ -axis points out the left ear, the  $y$ -axis out of the back of the head and the  $z$ -axis to the top. Thereby the plane of the horizontal semicircular canals and the  $x$ - $y$ -plane coincide. Since the measurements by Takagi and Sando also included the semicircular canals, it was possible to use their orientation together with the measured orientation of the canals (Blanks et al., 1975) to adjust the surfaces with a sequence of rotations. The resulting epithelia surfaces are shown in Fig. 1.

The relation between the direction of morphological polarization vectors in man and their location on the epithelia was described qualitatively in 2D by Lindeman (1969). Thus for every location on the epithelia the direction of the corresponding vector is approximately known.

We assume that the planes in which he represented the polarization vectors correspond to the  $x$ - $y$ -plane (as defined above) for the utricle, and the  $y$ - $z$ -plane for the saccule. Due to this assumption and the 2D representation, Lindemañs polarization vectors of the utricle possess no  $z$ -component in the 3D coordinate system and the saccule no  $x$ -component. As mentioned above, our approach is based on the supposition that morphological polarization vectors lie in tangent planes of the epithelia surfaces. Therefore, Lindemañs vectors need to be projected onto the curved epithelia. To this end, tangent planes on the regular grid were determined (Fig. 2A). The tangent planes are characterized by basis vectors. A basis vector  $\vec{u}$  at the location  $\mathbf{i}, \mathbf{j}$  was calculated from the difference of the surface points  $\mathbf{s}(\mathbf{i}, \mathbf{j} - \mathbf{1})$  and  $\mathbf{s}(\mathbf{i}, \mathbf{j} + \mathbf{1})$ . Similarly a basis vector  $\vec{v}$  was obtained from the points  $\mathbf{s}(\mathbf{i} - \mathbf{1}, \mathbf{j})$  and  $\mathbf{s}(\mathbf{i} + \mathbf{1}, \mathbf{j})$ . These basis vectors are generally not orthogonal. The projection  $\vec{p}_{\parallel}$  of a vector  $\vec{p}$  onto the surface can then be constructed using  $\vec{u}$  and  $\vec{v}$  (Fig. 2B):  $\vec{p}_{\parallel} = \alpha\vec{u} + \beta\vec{v}$ . A second vector  $\vec{p}_{\perp}$ , perpendicular to the surface can be found by forming the cross product of  $\vec{u}$  and  $\vec{v}$ :  $\vec{p}_{\perp} = \gamma\vec{u}\times\vec{v}$ . Because of the vector relation  $\vec{p} = \vec{p}_{\parallel} + \vec{p}_{\perp}$ , three equations exist to determine the three unknowns  $\alpha$ ,  $\beta$  and  $\gamma$ . After setting the length of the obtained tangent plane vector to unity, the vector was considered as the representation of the morphological vectors contained in the corresponding surface quadrilateral.

Lindeman depicted polarization vector patterns, using only a small number (<20) of vectors in the graphical displays. While this is sufficient to clarify the general distribution of morphological vectors, a much larger number is required to determine vector distributions. The vectors were set in a way that reproduces the findings by Lindeman and interpolates between his vectors in the remaining area. To simplify the task of setting the vectors, we created a graphical user interface that allowed interactive control over the orientation of the vectors, and automatically projected them onto the corresponding tangent plane on the

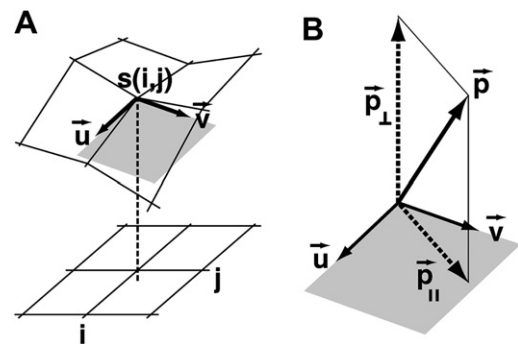


Fig. 2. Projection of the Lindemañs 2D vectors onto the curved epithelia surfaces. The curved surfaces are described by the function  $\mathbf{s}(\mathbf{i}, \mathbf{j})$  on a regular grid with coordinates  $\mathbf{i}$  and  $\mathbf{j}$  (A). Basis vectors  $\vec{u}$  and  $\vec{v}$  of a local tangent plane (gray) are calculated from the change of the surface around  $\mathbf{s}(\mathbf{i}, \mathbf{j})$ . Using these basis vectors, an arbitrary vector  $\vec{p}$  (for example a Lindemañ vector) can be split into a part  $\vec{p}_{\parallel}$ , lying in the tangent plane and a second part  $\vec{p}_{\perp}$ , perpendicular to it (B).

epithelium. Approximately 3000 polarization vectors were generated for the utricle and 2000 for the saccule. These numbers were determined by the grid-representation of the epithelia since every surface quadrilateral corresponded to one vector. On the utricle a vector represents the hair cells in an area of about  $3.3 \times 10^{-3} \text{ mm}^2$ , while on the saccule this area is about  $2.1 \times 10^{-3} \text{ mm}^2$ . Due to the curved shape of the epithelia the size of these areas shows some variation. Since about 8000 hair cells are found on the epithelia per square millimeter (Rosenhall and Rubin, 1975; Watanuki and Schuhknecht, 1976), a surface quadrilateral contains about 26 hair cells at the utricle and 17 at the saccule.

Next we determined how the computed polarization vectors are distributed over the unit sphere. To this end a set of vectors was constructed that covers all directions and could conveniently be used to create distribution plots. First the surface of a unit sphere is approximated with small planar areas, quadrilaterals in our case (Fig. 3A). Thereby the size of the areas varies, depending on the latitude. The spatial resolution was 80 steps for both, latitude and longitude. Next the center of each quadrilateral is determined from the four corner vertices, as shown in Fig. 3A. All vectors  $\vec{d}$  from the origin of the sphere to the centers of the quadrilaterals can be viewed as the discrete set of directions, which is used to classify the computed polarization vectors. Each center serves as the origin of a sphere with radius  $R$  (R-sphere), which has the same size for all quadrilaterals (Fig. 3B). Because every R-sphere encompasses the same fraction of the surface of the unit sphere, the varying areas of the quadrilaterals do not interfere with the vector distribution. If a polarization vector ends inside a particular R-sphere (like  $\vec{x}$  in Fig. 3B), it is associated with the quadrilateral, otherwise not.

As the size of these areas varies, adding up the number of polarization vectors which end in a particular R-sphere

does not yet yield an adequate vector distribution: each vector represents the hair cells in a small part of the epithelium, and by just counting vectors, a smaller area would be treated in the same way as a larger one. To overcome this difficulty, we simply added the size of the epithelia parts that correspond to the vectors. A vector density on the unit sphere can then be defined, which is the size of the summed epithelia areas, divided by the fraction of the unit-sphere surface, encompassed by an R-sphere.  $R$  needed to be chosen carefully since a large value smears out the distribution and leads to multiple counts of a vector, i.e. a vector is associated with several quadrilaterals. A small  $R$  results in vectors that do not contribute to any quadrilateral. Based on a radius of 1.0 for the vector distribution sphere, we chose a value of 0.08 for  $R$ . As long as  $R$  is small compared to 1.0, the angle  $\delta$  (Fig. 3B) is an alternative way to express the size of the R-sphere. Commonly, errors associated with the measurement of polarization vectors are given in terms of this angle and  $R = 0.08$  corresponds approximately to the magnitude of measurement errors of  $5^\circ$  (Fernandez and Goldberg, 1976a). The resulting distribution of polarization vectors on the unit sphere can now be visualized by coloring each quadrilateral in accordance to the epithelium area which it represents.

### 3. Results

Based on the measurements by Takagi and Sando and hair cell polarization vectors derived from the observations of Lindeman, we obtained the vector distributions presented in Fig. 4. This figure shows stereographic projections of the unit sphere, with the “north pole” of the sphere corresponding to a direction that points out of the top of the head, and the “south pole” out of the bottom. The equatorial plane coincides with the planes of the lateral semicircular canals. The number of polarization vectors that point into a particular direction, based on the R-sphere concept, i.e. the vector density, is color coded: “dark” indicates a high density, “light” a low density. Superimposed on the projections, Fig. 4 also shows polarization vectors that were found experimentally in single cell recordings from the vestibular nerve of squirrel monkeys (Fernandez and Goldberg, 1976a). Measured and modeled polarization vectors both emanate from epithelia on the left side of the head.

On the saccule (Fig. 4, right column) the highest vector density is found in two elliptic spots close to the northern and southern pole of the unit sphere. The corresponding hair cells are located in the lower part of the epithelium. The highest density on the utricle is found in the left upper quadrant of Fig. 4A. A particular large number of utricular polarization vectors point straight ahead. Maximum vector densities are similar on the utricle and the saccule. There are also extended regions where the vector density is barely above zero. Densities did not show any apparent symmetry apart from the spots of the saccule, left and right of the mid-sagittal plane.

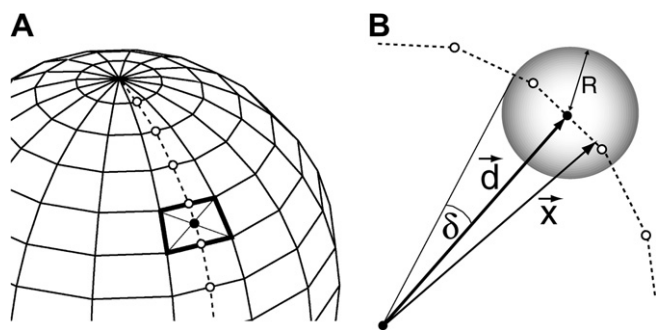


Fig. 3. Approximation of the unit sphere, construction of the direction vectors and R-sphere. (A) The planar quadrilaterals used for the approximation of the unit sphere. The center of one quadrilateral is indicated by a filled circle. (B) A section through the unit sphere. The section runs along the dashed line in (A). Borders of quadrilaterals are indicated with open circles. Members of the direction set vectors  $\vec{d}$  point to the centers of the quadrilaterals. Polarization vectors  $\vec{x}$  are associated with a particular direction if they point to a location inside a sphere with radius  $R$  around the tip of  $\vec{d}$ . The angle  $\delta$  represents an alternative way to indicate the size of the R-sphere.

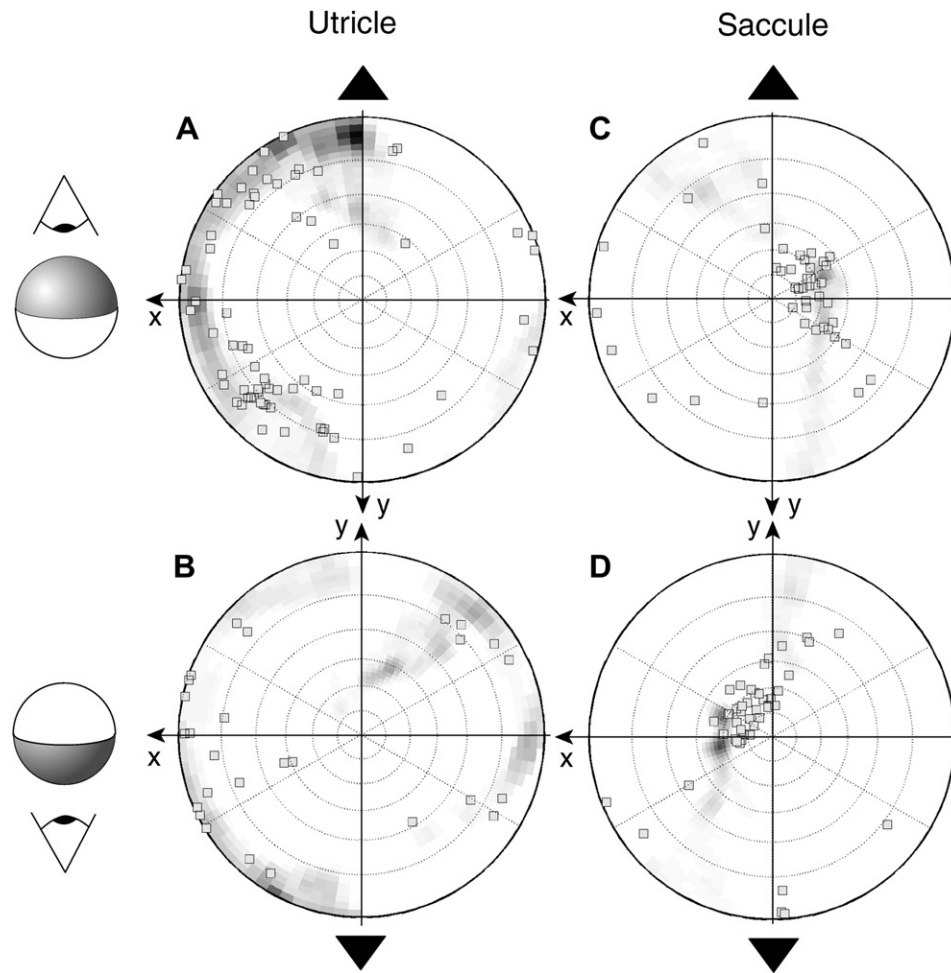


Fig. 4. Projections of the calculated morphological vector distribution and measured functional polarization vectors (Fernandez and Goldberg, 1976a) of left utricle (A/B) and saccule (C/D). Vector densities increase from white over gray to black. They were normalized with respect to the largest density found on one of the epithelia. Black filled triangles outside the circles indicate the direction of the nose, and the sketches on the left illustrate the view on the hemispheres: upper hemisphere in the upper row and lower hemisphere in the lower row. Concentric coordinate circles correspond to steps of 15°.

Assuming that the measurements of vestibular polarization vectors are not biased towards certain directions and that the sample is large enough, it is possible to compare the predicted and the measured polarization vector distributions. For the utricle (left column in Fig. 4), the model predicts that most vectors point in the left, frontal direction (Fig. 4A, left, upper quadrant and 4B, left, lower quadrant) and in fact a considerable number of measured superior nerve units have this property (33 out of 97 afferents). Surprisingly, an even larger number of afferent units (45) point into the left posterior direction (Fig. 4A, left lower quadrant and 4B, left upper quadrant). For the saccule (right column), the model predicts that most of the polarization vectors point into two strongly elliptic regions close to the  $z$ -axis of the head fixed coordinate system. This prediction is confirmed by the measurements in the inferior nerve (Figs. 4C and D) though the vectors are distributed over a larger region.

While most experimentally recorded afferent vectors point into directions that are also covered by computed polarization vectors, there are also vectors outside the

expected areas. For example, several data points in the left part of Fig. 4C have a large positive  $x$ -component and do not fall onto shaded areas. Since the saccule is predominantly oriented in the  $y$ - $z$ -plane, its functional polarization vectors should be close to this plane too, regardless of how morphological vectors are oriented on the epithelium. Interestingly a large number of utricular polarization vectors can be found that point into this direction (Fig. 4A).

A different way of looking at the same data can be obtained by ignoring the vector densities, and coloring all areas uniformly gray, that possess a non-zero density. This results in the middle and lower plots of Fig. 5, which indicate all directions covered by hair cell polarization vectors. The plots also include directions of some vectors at “prominent” locations on the epithelia. The locations of the points u1–u8 on the utricular (Fig. 5A) and s1–s9 on the saccular (Fig. 5D) macula are indicated in the middle and lower rows of Fig. 5. Apart from the direction change across the MRL, hair cell polarization vectors from bordering regions on the epithelium typically point into similar

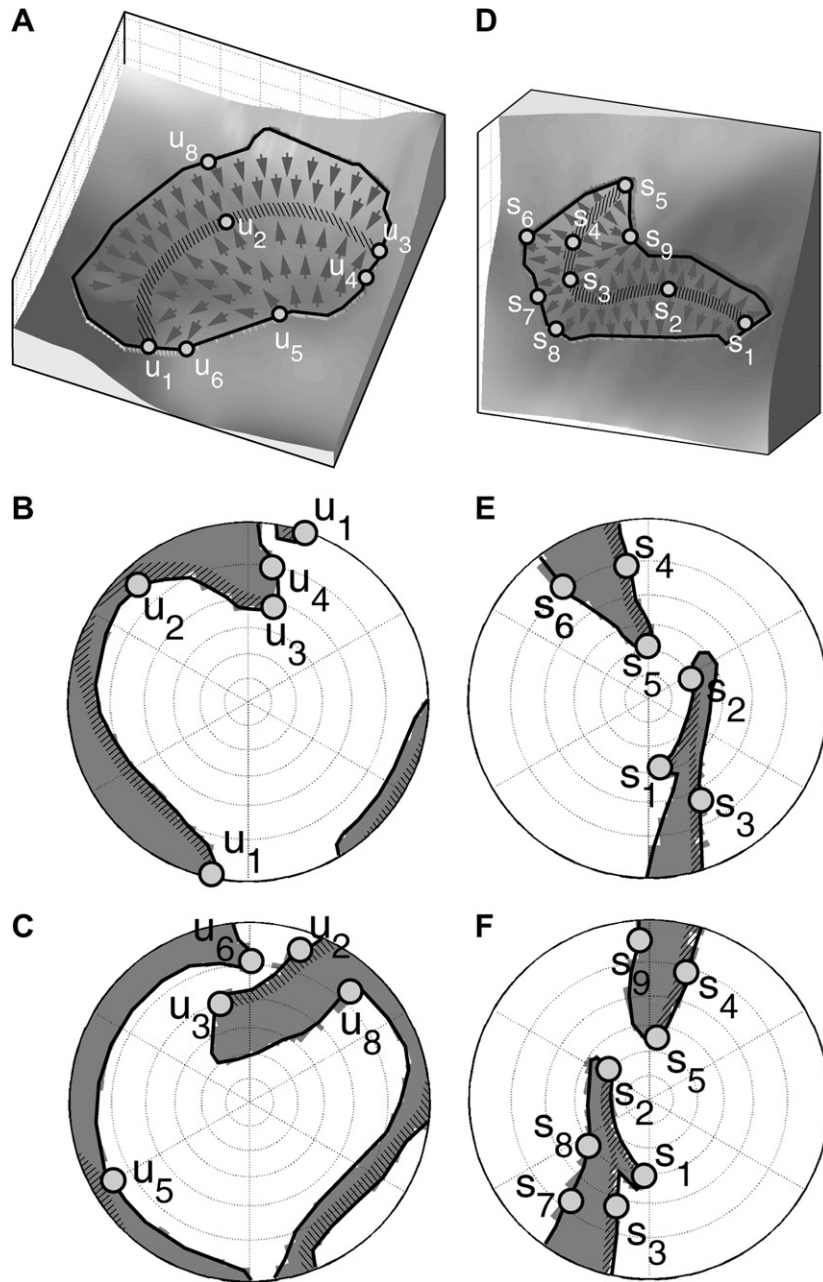


Fig. 5. Relation between the location of hair cells on the epithelia and the direction of their polarization vectors. A limited number of hair cells at prominent locations of left utricle (A) and saccule (D) is considered here. Locations are termed u1–u8 on the utricle and s1–s9 on the saccule and marked with open circles. The wide hatched lines indicate the positions of the MRLs. The direction of computed polarization vectors, that correspond to these locations are shown in (B/C) for the utricle and (E/F) for the saccule. The coordinate system is identical to the one used in Fig. 4, i.e. upper hemisphere in the upper row and lower hemisphere in the lower row. Like in the pictures of the epithelia (A/D), directions are indicated by open circles named u1–u8 for the utricle and s1–s9 for the saccule. Also, the direction of hair cells along the MRLs are shown as wide hatched lines. All directions that are covered by polarization vectors from the entire epithelia are colored uniformly gray, without regard to the vector density. The direction of polarization vectors that correspond to locations on the MRL like u1 or s2 appear two times: One for each direction that occurs in this region. The wide hatched lines of the MRLs are treated in the same way.

directions in space. Accordingly, hair cell polarization vectors from the band-like MRL are associated with a band-like distribution of polarization vectors on the sphere. This does not imply a unique mapping of macular regions to areas on the sphere. Since the direction of polarization vectors flips by 180° within the MRL, points from this region appear two times.

#### 4. Discussion

The calculated distributions of morphological polarization vectors presented above have allowed us to make a direct comparison with afferent nerve recordings. As expected from the orientation of the epithelia and the assumption that morphological polarization vectors lie in

tangent planes of them, our model yields results that show substantial similarity to the distribution of functional vectors obtained from measurements. It predicts that morphological polarization vectors of the utricle lie approximately in the plane of the lateral semicircular canals, while saccular vectors are close to the mid-sagittal plane.

But there are also some marked differences between modeled and measured polarization vectors. Measurement errors associated with the direction of functional vectors are rather small and should not exceed 5° (Fernandez and Goldberg, 1976a). They may play a role in the distribution of functional vectors around the northern and southern “spot” of the saccule, since modeling suggests that these spots should be smaller (Figs. 4C/D). Another source of errors may be related to the identification of vestibular units. They are usually assigned to the utricular or saccular epithelium if they are found in the upper or lower part of the vestibular nerve, respectively. Such assignment errors might for instance have occurred in the case of the functional vectors visible in the lower left quadrant of Fig. 4C. If these vectors were attributed to the utricle, they would be situated in the lower left quadrant of Fig. 4A, a direction in which a lot of utricular vectors point.

Based on geometric and mechanical aspects of the otolith membrane, it has been proposed that functional polarization vector are composed from contributions of terminal field members with substantially different properties (Kondrachuk, 2001). Three observations support this argument: (1) It has been found that there are more utricular afferents with vectors pointing to the ipsi- than to the contralateral side (Fernandez and Goldberg, 1976a; Goldberg et al., 1990a). The finding has been attributed to the relative size of areas which house ipsi- and contralateral morphological vectors, but this could not account for the full extent of the observation (Goldberg et al., 1990a). (2) Spatio-temporal convergence was observed in some afferent fibers (Dickman et al., 1991). This also suggests that hair cells with substantially different morphological polarization vectors are involved in the formation of the afferent response. (3) Structures have been identified that might be responsible for intra-epithelial information transport (Sans et al., 2001). Because of these observations, it cannot be ruled out, that the direction of functional polarization vectors is systematically influenced by such a mechanism. The most likely observation related to this kind of processing is the discrepancy between measured and modeled utricular vectors in Fig. 4A, upper and lower left quadrant.

Both foundations of the model, the shapes of the epithelia and the distribution patterns of morphological polarization vectors over them, are subject to errors. Shapes were found by a complicated slicing procedure and subsequent processing of the resulting geometrical data. This yields reconstructed shapes that will not exactly coincide with the original shapes. And for the hair cell polarization vectors, several publications exist where the distribution of morphological vectors are depicted qualitatively (Flock,

1964; Fluor, 1969; Lindeman, 1969; Rosenhall, 1972). To our knowledge, the direction of morphological vectors has never been determined on a quantitative basis. Unfortunately considerable variations exist between the observations of different authors with regard to the shape of the epithelia as well as the patterns of polarization vector distributions. From this it can be expected that polarization vectors and their relation to locations on the epithelia is only known with limited accuracy. Also the experiments which form the basis of this investigation were performed on different individuals of the same species as well as in different species. Specifically the shape of the epithelia was measured in man, while functional polarization vectors were determined in monkeys. Due to their different movement repertoire it is reasonable to assume that an optimization of the balance system with respect to these repertoires, lead to differently shaped epithelia. It might therefore be possible that the distribution differences in Fig. 4A, upper and lower left quadrant has such a cause. More experimental work is required to resolve the differences between the measured and modeled findings. A lot of exciting experimental and theoretical work is currently carried out in the understanding of the micro-mechanics of vestibular hair bundles (Nam et al., 2006; Kozlov et al., 2007), as well as in the local variations of different hair cell types (Xue and Peterson, 2006). While integration of this structural work with the 3D geometric properties of the otolith is very challenging, we believe that the representation presented above should facilitate the planning of neurophysiological experiments on the vestibular system, as well as the interpretation and understanding of the resulting data.

## Acknowledgments

This study was supported by the Betty and David Koetser Foundation for Brain Research and by DLR 50WB9940. Special thanks goes to Jay Goldberg, for providing his experimental data, and for the permission to use them in this publication.

## References

- Blanks, R.H., Curthoys, I.S., Markham, C.H., 1975. Planar relationships of the semicircular canals in man. *Acta Otolaryngol.* 80, 185–196.
- Curthoys, I.S., Betts, G.A., Burgess, A.M., MacDougall, H.G., Cartwright, A.D., Halmagyi, G.M., 1999. The planes of the utricular and saccular maculae of the guinea pig. *Ann. NY Acad. Sci.* 871, 27–34.
- Dickman, J.D., Angelaki, D.E., Correia, M.J., 1991. Response properties of gerbil otolith afferents to small angle pitch and roll tilts. *Brain Res.* 556, 303–310.
- Fernandez, C., Goldberg, J.M., 1976a. Physiology of peripheral neurons innervating otolith organs of the squirrel monkey. I. Response to static tilts and to long duration centrifugal force. *J. Neurophysiol.* 39 (5), 970–984.
- Fernandez, C., Goldberg, J.M., 1976b. Physiology of peripheral neurons innervating otolith organs of the squirrel monkey. II. Directional selectivity and force–response relations. *J. Neurophysiol.* 39, 985–995.

- Fernandez, C., Goldberg, J.M., Baird, R.A., 1990. The vestibular nerve of the chinchilla III. Peripheral innervation patterns in the utricular macula. *J. Neurophysiol.* 63, 767–780.
- Flock, A., 1964. Structure of the macula utriculi with special reference to directional interplay of sensory responses as revealed by morphological polarization. *J. Cell Biol.* 22, 413–431.
- Fluur, E., 1969. The interaction between the utricle and the saccule. *Acta Otolaryngol.* 69, 17–24.
- Goldberg, J.M., Desmadryl, G., Baird, R.A., Fernandez, C., 1990a. The vestibular nerve of the chinchilla IV. Discharge properties of utricular afferents. *J. Neurophysiol.* 63, 781–790.
- Goldberg, J.M., Desmadryl, G., Baird, R.A., Fernandez, C., 1990b. The vestibular nerve of the chinchilla. V. Relation between afferent discharge properties and peripheral innervation patterns in the utricular macula. *J. Neurophysiol.* 63, 791–804.
- Holstein, G.R., Rabbitt, R.D., Martinelli, G.P., Friedrich Jr., V.L., Boyle, R.D., Highstein, S.M., 2004. Convergence of excitatory and inhibitory hair cell transmitters shapes vestibular afferent responses. *Proc. Natl. Acad. Sci. USA* 101 (44), 15766–15771.
- Kachar, B., Parakkal, M., Fex, J., 1990. Structural basis for mechanical transduction in the frog vestibular sensory apparatus: I. The otolithic membrane. *Hear. Res.* 45 (3), 179–190.
- Kondrachuk, A.V., 2001. Simulation and interpretation of experiments with otoliths. *J. Gravit. Physiol.* 8 (1), 101–104.
- Kozlov, A.S., Risler, T., Hudspeth, A.J., 2007. Coherent motion of stereocilia assures the concerted gating of hair-cell transduction channels. *Nat. Neurosci.* 10, 87–92.
- Lindeman, H.H., 1969. Studies on the morphology of the sensory regions of the vestibular apparatus. *Ergeb. Anat. Entwicklungsgesch.* 42, 1–113.
- Nam, J.H., Cotton, J.R., Peterson, E.H., Grant, W., 2006. Mechanical properties and consequences of stereocilia and extracellular links in vestibular hair bundles. *Biophys. J.* 90, 2786–2795.
- Press, W.H., Teukolsky, S.A., Vetterling, W.T., Flannery, B.P., 1992. *Numerical Recipes*, second ed. Cambridge.
- Rosenhall, U., 1972. Vestibular macular mapping in man. *Ann. Otol.* 81, 339–351.
- Rosenhall, U., Rubin, W., 1975. Degenerative changes in the human vestibular sensory epithelia. *Acta Otolaryngol.* 79, 67–80.
- Ross, M., 1985. Anatomical evidence for peripheral neural processing in mammalian graviceptors. *Aviat. Space Environ. Med.* 56, 338–343.
- Sans, A., Dechesne, C.J., Demêmes, D., 2001. The mammalian otolithic receptors: a complex morphological and biochemical organization. In: Tran Ba Huy, P., Toupet, M. (Eds.), *Otolith Functions and Disorders*, *Advances in Otorhinolaryngology* Basel, vol. 58. Karger, pp. 1–14.
- Shotwell, S.L., Jacobs, R., Hudspeth, A.J., 1981. Directional sensitivity of individual vertebrate hair cells to controlled deflection of their hair bundles. *Ann. NY Acad. Sci.* 374, 1–10.
- Takagi, A., Sando, I., 1988. Computer-aided three-dimensional reconstruction and measurement of the vestibular end-organs. *Otolaryngol. Head Neck Surg.* 98 (3), 195–202.
- Tribukait, A., Rosenhall, U., 2001. Directional sensitivity of the human macula utriculi based on morphological characteristics. *Audiol. Neuro-Otol.* 6, 98–107.
- Watanuki, K., Schuhknecht, H.F., 1976. A morphological study of human vestibular sensory epithelia. *Arch. Otolaryngol.* 102, 583–588.
- Xue, J., Peterson, E.H., 2006. Hair bundle heights in the utricle: differences between macular locations and hair cell types. *J. Neurophysiol.* 95, 171–186.